Effect of Ionic Sizes on the Electrokinetic Flow in a Planar Slit Covered by an Ion-Penetrable Charged Membrane

Jyh-Ping Hsu* and Shih-Wei Huang

Department of Chemical Engineering, National Taiwan University, Taipei, Taiwan 10617, Republic of China

Shiojenn Tseng

Department of Mathematics, Tamkang University, Tamsui, Taipei 25137, Republic of China

Received: September 26, 2002; In Final Form: October 30, 2002

The electrokinetic flow in a planar slit covered by an ion-penetrable charged membrane in an *a*:*b* electrolyte solution, taking the effect of the sizes of charged species into account, is analyzed theoretically. The electrokinetic properties such as volumetric flow rate, total electric current, and streaming potential of the system under consideration are evaluated. The influences of the key parameters, which include the frictional coefficient of the membrane layer, membrane thickness, ionic strength, valence of counterions, fixed charge concentration, and sizes of cations and anions, are discussed. We demonstrate the importance of the steric ionic effects by showing that a substantial difference between the classic point-charge model and the present model.

1. Introduction

The flow of an electrolyte solution in a microchannel driven by an applied electric field and/or pressure gradient has wide applications in both industrial and biomedical processes, for example, design of microfluidic systems, microheat sinks used in electronic cooling, flow of fluid in organic bodies, and biomedical diagnostic instruments. In contrast to the flow of fluid in a macro-channel, if the characteristic dimension of a channel if of micrometer size, the behavior of fluid flow inside is strongly influenced by the electrical properties of channel wall, and the corresponding equations governing the flow behavior needs to be modified accordingly. The classical work of Smoluchowski[1] gives the basic description of the flow of an electrolyte solution through an infinitely wide pore. Early attempts to the flow through narrow capillaries were made by Dresner and Kraus.[2] Burgreen and Nakache[3] analyzed the electrokinetic flow in an ultrafine capillary slit by extending the classic theory, which is limited to the flow in a channel of large electrokinetic radius or to a bare-wall at low surface potentials. Rice and Whitehead[4] gave a Debye−Huckel correction for narrow cylindrical capillaries. Sørensen and Koefoed[5] evaluated all the electrokinetic phenomenological coefficients for capillaries with a circular cross section and a bare-wall fixed charge under Debye−Huckel conditions at all ratios between pore radius and Debye length. Hildreth[6] and Levine et al.[7] applied a nonlinear Poisson−Boltzmann equation to study the electrokinetic flow in a narrow slit. The flow of an electrolyte solution between two parallel plates, each is covered by an ion-penetrable membrane, was discussed by Donath and Voigt.[8] They showed that if the fixed charge in the membrane phase follows the distribution, which satisfies a minimum energy criterion, then the streaming current can be derived analytically.[9] Ohshima and Kondo[10] derived approximate expressions for electroosmotic velocity, volumetric flow rate, total current, and streaming potential by assuming uniform fixed charge distribution, large separation between two plates, and thick membrane. Tseng et al.[11] considered the flow of an electrolyte solution in a planar slit, the wall of which is covered by an ion-penetrable charged membrane. An approximate analytical expression for electrical potential was derived, and the behaviors of the electrokinectic phenomena were explored. Keh and Liu[12] examined the electrokinetic flow in a capillary with circular cross section, the wall of which is covered by a charged surface layer bearing uniformly distributed fixed charge, under the conditions of low electrical potential. They showed that, depending upon the characteristics of the electrolyte solution, the surface charge, the capillary geometry and the structure of the surface layer, either an augmented or a diminished electrokinetic flow relative to the flow in a bare-wall capillary might be observed.

The results discussed above are based on the classic Gouy−Chapman theory[1] in which ionic species are treated as point charges, that is, the effect of their sizes on the behavior of the system under consideration is neglected. This theory was modified by Stern[1] to introduce the steric effects by excluding the ions from the first molecular layer close to a charged surface. Henderson and Blum[13] proposed a modified Stern model for electrolyte ions near an interface. Torrie and Valleau[14] applied a Monte Carlo simulation to justify the applicability of this model. On the basis of the model of Henderson and Blum,[13] Valleau and Torrie[15] and Bhuiyan et al.[16] concluded that the effective sizes of mobile ions play a significant role in the description of the nature of the electrical double layer surrounding a charged surface. The effect of ionic sizes on the properties of electrical double layer was also investigated through statistical mechanics approach.[17−19] Gonzalez-Tovar et al.[20] used a hypernetted chain-mean-spherical integral equation to calculate several electrokinetic quantities for a 1:1 electrolyte solution in a charged slit by taking into account the ionic sizes. The effects of ionic sizes on the double layer properties[21−25] and on

* To whom correspondence should be addressed. Fax: 886-2-23623040. E-mail: jphsu@ccms.ntu.edu.tw.

10.1021/jp0270699 CCC: $25.00
Published on Web 12/03/2002

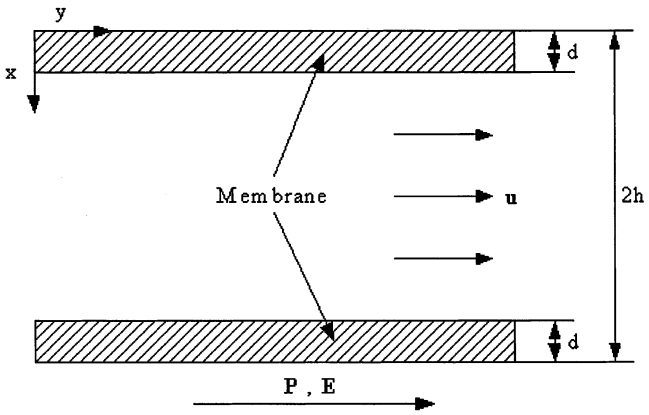

Figure 1. Schematic representation of the system under consideration where a planar slit, which comprises two planar, parallel, rigid plates each is covered by an ion-penetrable membrane of thickness *d*. 2*h* is the separation distance between plates, **u** is the velocity of the electrolyte solution, **E** is the applied electrical field, and **P** is the gradient of applied pressure *p*.

the electrokinetic behavior[26,27] for particles covered by an ion-penetrable membrane were also discussed in the literature.

In the present study, the electrokinetic flow of an electrolyte solution in a planar slit covered by an ion-penetrable charged membrane is investigated taking the sizes of all the charged species into account. These results are compared to those obtained through the Poisson−Boltzmann equation for a point charge model (PCM).

2. Modeling

The problem under consideration is shown in Figure 1. We consider a steady flow of an incompressible *a*:*b* electrolyte solution in a planar slit, which comprises two identical, rigid, planar parallel plates each is covered by an ion-penetrable membrane layer of scaled thickness *d* carrying uniformly distributed fixed charge of concentration N_0. The scaled separation distance between two plates is 2*h*. The Cartesian coordinates are chosen so that its origin is on the plate-membrane interface, and the flow of liquid is in the *y*-direction. A uniform electrical field **E** with strength $E = -\partial\varphi/\partial y$ and a uniform pressure gradient **P** with magnitude $P = -\partial p/\partial y$ are applied in the direction of the flow of the liquid phase, φ and p being respectively the electrical potential and the pressure. Suppose that the fixed charge in the membrane layer is negative with valence *z*. Because the geometry under consideration is symmetric to *y*-axis, only the domain $0 < X < h$ needs to be considered, *X* being the scaled distance in the *x*-direction. Denote the effective radii of fixed charged groups, anions (coions), and cations (counterions) as σ_f, σ_{an}, and σ_{ca} respectively. For convenience, we assume that $\sigma_f > \sigma_{an} > \sigma_{ca}$. Other possible cases can be analyzed in a similar way.

The problem under consideration involves solving simultaneously the electric field and the flow field. Figure 2 shows the arrangement of the charged species in the membrane layer where the margin of the leftmost fixed charged group coincides with the plate-membrane interface, and that of the rightmost one coincides with the membrane-liquid interface.[23] The scaled symbols are defined by $X = \kappa x$, $X_{ca} = \kappa\sigma_{ca}$, $X_{an} = \kappa\sigma_{an}$, $X_i = \kappa\sigma_f$, and $X_o = d - \kappa\sigma_f$, where κ and *x* are the reciprocal Debye length and the distance from the rigid plate, respectively. The cross section of the microchannel is divided into five regions. Region I ($X < X_{ca}$) contains the charge-free region ($-\infty < X < 0$) and the inner uncharged membrane ($0 < X < X_{ca}$), *X* is the scaled distance. Region II ($X_{ca} < X < X_{an}$) has cations only.

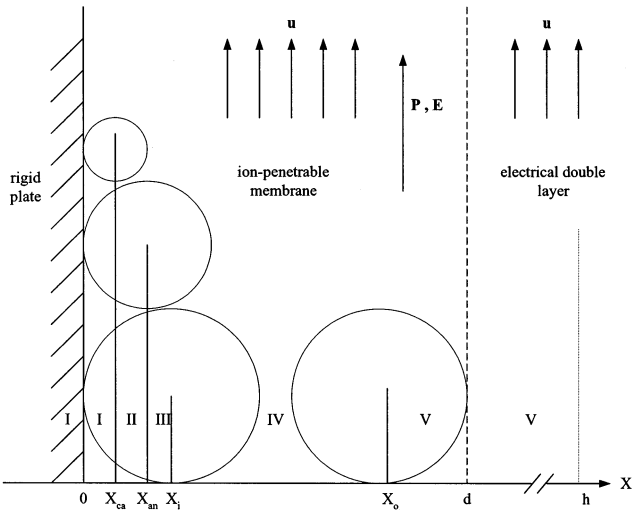

Figure 2. Schematic representation of the system under consideration. X_{ca}, X_{an}, X_i, X_o, and *d* are respectively scaled locations of the effective most interior locations of positive and negative charges, the locations of inner plane of the fixed charge and outer plane of fixed charge, and the scaled thickness of the membrane. The scaled size of fixed charged group is X_i. Regions I−V denote respectively the charge-free region, the region in which only cations are present, the region in which both cations and anions are present, the region in which all charged species are present, and the region which comprise the outer uncharged membrane and the diffuse double layer.

Region III ($X_{an} < X < X_i$) has both cations and anions. Region IV ($X_i < X < X_o$) contains all charged species, and region V ($X_o < X$), which comprises the outer uncharged membrane ($X_o < X < d$) and the liquid phase up to the center of the microchannel ($d < X < h$). Here, X_{ca} and X_{an} are the most interior locations of positive and negative charges respectively, and X_i and X_o represent the locations of the inner plane of fixed charge and the outer plane of fixed charge, respectively. X_i is the effective scaled radius of fixed charged group.

The electrical potential is described by the modified Poisson−Boltzmann equation

$$\frac{d^2\psi}{dX^2} = 0, \quad \text{region I} \tag{1}$$

$$\frac{d^2\psi}{dX^2} = \frac{-\exp(-a\psi)}{a+b}, \quad \text{region II} \tag{2}$$

$$\frac{d^2\psi}{dX^2} = \frac{-\exp(-a\psi) + \exp(b\psi)}{a+b}, \quad \text{region III} \tag{3}$$

$$\frac{d^2\psi}{dX^2} = \frac{-\exp(-a\psi) + \exp(b\psi) + N}{a+b}, \quad \text{region IV} \tag{4}$$

$$\frac{d^2\psi}{dX^2} = \frac{-\exp(-a\psi) + \exp(b\psi)}{a+b}, \quad \text{region V} \tag{5}$$

In these expressions, $\psi = F\phi/RT$, $\kappa^2 = F^2[a(a+b)C_a^0]/\epsilon_0\epsilon_r RT$, $aC_a^0 = bC_b^0$, and $N = zN_0/aC_a^0$, where ϕ is the electrical potential; C_a^0 and C_b^0 are the concentrations of ionic species of valences *a* and *b* in the bulk liquid-phase respectively; *F*, *R*, and *T* are respectively the Faraday constant, the gas constant, and the absolute temperature; ϵ_r and ϵ_0 are the relative permittivity of the electrolyte solution and the permittivity of a vacuum, respectively. The relative permittivity of the membrane and that of the liquid phase are assumed to be constant.

The boundary conditions associated with eqs 1−5 are

$$\frac{d\psi}{dX} \to 0 \qquad \text{as} \qquad X \to 0 \qquad \text{and} \qquad X \to h \tag{6}$$

$$\left(\frac{d\psi}{dX}\right)_{X=X_{ca}^{+}} = \left(\frac{d\psi}{dX}\right)_{X=X_{ca}^{-}} \qquad \text{and} \qquad \psi(X_{ca}^{+}) = \psi(X_{ca}^{-}) \tag{7}$$

$$\left(\frac{d\psi}{dX}\right)_{X=X_{an}^{+}} = \left(\frac{d\psi}{dX}\right)_{X=X_{an}^{-}} \qquad \text{and} \qquad \psi(X_{an}^{+}) = \psi(X_{an}^{-}) \tag{8}$$

$$\left(\frac{d\psi}{dX}\right)_{X=X_{i}^{+}} = \left(\frac{d\psi}{dX}\right)_{X=X_{i}^{-}} \qquad \text{and} \qquad \psi(X_{i}^{+}) = \psi(X_{i}^{-}) \tag{9}$$

$$\left(\frac{d\psi}{dX}\right)_{X=X_{o}^{+}} = \left(\frac{d\psi}{dX}\right)_{X=X_{o}^{-}} \text{and } \psi(X_{o}^{+}) = \psi(X_{o}^{-}) \tag{10}$$

These conditions are based on the assumptions that the electric field is absent in the rigid plate, and both the electrical and its gradient are continuous at the intersection of two adjacent regions.

We assume that the flow field can be described by the Navier−Stokes equation[10]

$$\frac{d^2U}{dX^2} - \eta^*\lambda^2 U = \eta^* H, \quad 0 < X < X_{ca} \tag{11}$$

$$\frac{d^2U}{dX^2} - \eta^*\lambda^2 U = \eta^* L\frac{-\exp(-a\psi)}{a+b} - \eta^* H, \quad X_{ca} < X < X_{an} \tag{12}$$

$$\frac{d^2U}{dX^2} - \eta^*\lambda^2 U = \eta^* L\frac{-\exp(-a\psi) + \exp(b\psi)}{a+b} - \eta^* H, \quad X_{an} < X < d \tag{13}$$

$$\frac{d^2U}{dX^2} = L\frac{-\exp(-a\psi) + \exp(b\psi)}{a+b} - H, \quad d < X < h \tag{14}$$

In these expressions, $U = u/u_0$, $\eta^* = \eta_s/\eta_m$, $\lambda^2 = f/\eta_s\kappa^2$, $L = \epsilon_0\epsilon_r RTE/\eta_s e u_0$, and $H = P/\eta_s\kappa^2 u_0$, where u_0 is a reference velocity, η_s and η_m are respectively the viscosity of the liquid phase and that of the membrane phase, and f is the friction coefficient of the membrane layer. The slipping plane is located at the rigid plate-membrane interface. Suppose that both the velocity and the tangential component of the stress tensor are continuous at the closet approach of cations X_{ca}, the closet approach of anions X_{an}, and the membrane−liquid interface d. Therefore the boundary conditions associated with eqs 11−14 are

$$U = 0 \qquad \text{as} \qquad X \to 0 \tag{15}$$

$$\left(\frac{dU}{dX}\right)_{X=X_{ca}^{-}} = \left(\frac{dU}{dX}\right)_{X=X_{ca}^{+}} \qquad \text{and} \qquad U(X_{ca}^{-}) = U(X_{ca}^{+}) \tag{16}$$

$$\left(\frac{dU}{dX}\right)_{X=X_{an}^{-}} = \left(\frac{dU}{dX}\right)_{X=X_{an}^{+}} \qquad \text{and} \qquad U(X_{an}^{-}) = U(X_{an}^{+}) \tag{17}$$

$$\left(\frac{dU}{dX}\right)_{X=d^{-}} = \eta^*\left(\frac{dU}{dX}\right)_{X=d^{+}} \qquad \text{and} \qquad U(d^{-}) = U(d^{+}) \tag{18}$$

$$\frac{dU}{dX} = 0 \qquad \text{as} \qquad X \to h \tag{19}$$

Once the electric field and the velocity field are determined, basic properties of the system under consideration such as the volumetric flow rate, the electric current, and the streaming potential can be evaluated. The scaled volumetric flow rate V can be calculated by

$$V = \frac{v}{u_0/\kappa} = 2\int_0^h U(X)\, dX \tag{20}$$

where v is the volumetric flow rate. The electric current density $i(x)$ can be evaluated by

$$i(x) = aFC_a(x)v_a(x) - bFC_b(x)v_b(x) \tag{21}$$

where C_a and C_b are respectively the concentrations of cations and anions, and v_a and v_b are the corresponding velocities. The electrochemical potentials of cations and anions μ_a and μ_b can be expressed respectively as[10]

$$\mu_a(x,y) = \mu_{a0} + ae\psi(x,y) + k_B T\ln[C_a(x)] \tag{22a}$$

and

$$\mu_b(x,y) = \mu_{b0} - be\psi(x,y) + k_B T\ln[C_b(x)] \tag{22b}$$

where μ_{a0} and μ_{b0} are constant, and k_B is the Boltzmann constant. The velocity of ion species i v_i can be expressed as[10]

$$v_i(x) = u(x) - \frac{1}{f_i}\frac{\partial}{\partial y}\mu_i(x,y), \tag{23}$$

where f_i is the drag coefficient of ionic species i. Equations 21−23 yield

$$i(x) = \frac{FzN_0}{N}\left\{-Gu_0U(X) + \frac{FE}{N_A}\left[\frac{a}{f_a}\exp(-a\psi) + \frac{b}{f_b}\exp(b\psi)\right]\right\} \tag{24}$$

where $G = -\exp(-a\psi) + \exp(b\psi)$, N_A being the Avogadro number. The total electric current in the y-direction I_t can be evaluated by

$$I_t = 2\int_0^h i(x)\, dx = \frac{2}{k}\int_0^h i(X)\, dX \tag{25}$$

The streaming potential E_{st} is the value of E when $I_t = 0$.

TABLE 1: Values of the Scaled Volumetric Flow Rate V and the Total Current I_t at Various η^*[a]

	η^*					
	1	1/2	1/5	1/10	1/20	1/50
V	3860	2111	901	461.5	233.7	94.18
I_t ($\times 10^{-6}$A)	1.593	1.585	1.578	1.576	1.575	1.574

[a] Parameters used are $T = 298$ K, $\epsilon_r = 78.5$, $I = 10^{-4}$ M, $\eta_s = 8.91 \times 10^{-4}$ Ns/m^2, $f = 10^{12}$ Ns/m,^{4} $d = 1$, $h = 10$, $a = b = 1$, $z = 1$, $N_0 = 5 \times 10^{-4}$ M, $E = 800$ V/m, $P = 0$ N/m^3, $f_a = f_b = 10^{-12}$ kg/s, $u_0 = 10^{-7}$m/s, $X_{ca} = 0.05$, $X_{an} = 0.1$, and $X_i = 0.2$.

3. Results and Discussions

The behaviors of the system under consideration are investigated through numerical simulation. For illustration, we assume that the negative fixed charge in membrane layer has $z = 1$. Table 1 shows the values of the scaled volumetric flow rate V and the total current I_t at various values of η^* (=viscosity of liquid phase/viscosity of membrane phase) for the case when pressure gradient is not applied. This table reveals that both V and I_t increase with the increase in η^*. This is because a small η^* implies that the viscosity of the membrane phase is large,

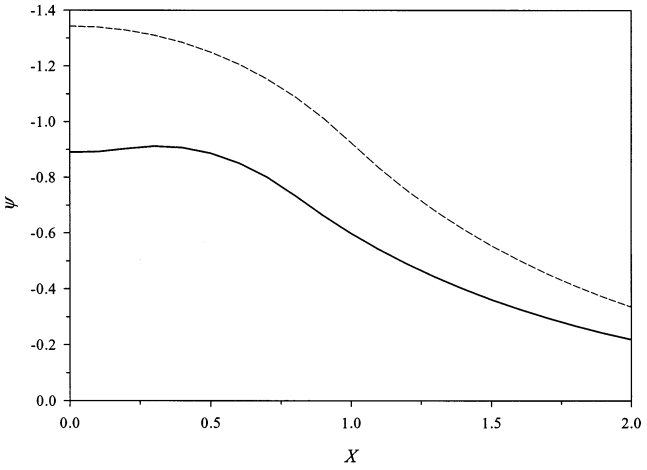

Figure 3. Variation of scaled potential ψ as a function of scaled distance X. Solid curve, present model, dashed curve, PCM. Key: $T = 298$ K, $\epsilon_r = 78.5$, $I = 10^{-4}$ M, $\eta_s = 8.91 \times 10^{-4}$ Ns/m^2, $f = 10^{12}$ Ns/m,^{4} $d = 1$, $h = 10$, $a = b = 1$, $z = 1$, $N_0 = 5 \times 10^{-4,}$ M, $E = 800$ V/m, $P = 0$ N/m^3, $f_a = f_b = 10^{-12}$ kg/s, $u_0 = 10^{-7}$m/s, $\eta^* = 1$, $X_{ca} = 0.05$, $X_{an} = 0.1$, and $X_i = 0.2$.

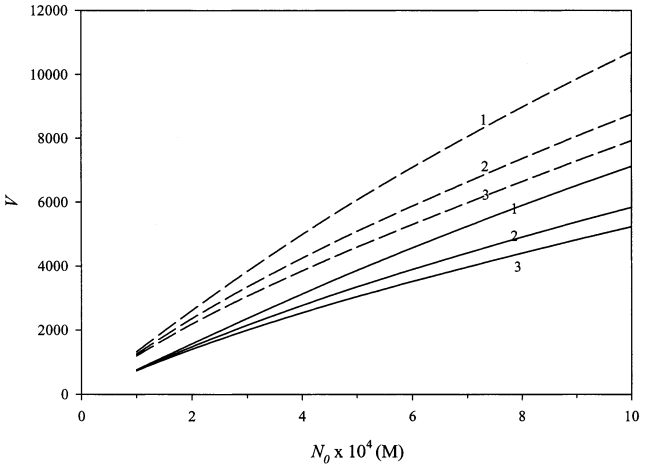

Figure 4. Variation of the scaled volumetric flow rate V as a function of fixed charge concentration N_0 at various valances of cations. Solid curves, present model, dashed curves, PCM. Curves 1, $a = 1$, $b = 1$; 2, $a = 2$, $b = 1$; 3, $a = 3$, $b = 1$. Key: same as in that in Figure 3 except for the values of a, b, and N_0.

which leads to a small flow rate inside. Note that the dependence of V on η^* is much more sensitive than that of I_t.

Figure 3 shows the simulated variation in the scaled electrical potential ψ as a function of the scaled distance X. For comparison, the corresponding result based on the classic point charge model (PCM) is also represented in this figure. Figure 3 reveals that $|\psi|$ exhibits a local maximum as X varies, which is not observed in the corresponding PCM where $|\psi|$ decreases monotonically with X. In general, the latter will overestimate $|\psi|$. This is because the fixed charge is present in region IV only in the present model, but it is present in the whole membrane layer in the corresponding PCM.

The variations of the scaled volumetric flow rate V and the total current I_t as a function of the concentration of fixed charge N_0 at various valences of cations (counterions) for the case pressure gradient is not applied are presented in Figures 4 and 5, respectively. Figures 4 and 5 reveal that, for a fixed ratio of (valence of cations/valence of anions), V and I_t all increase with an increase in N_0. This is expected since the higher the N_0, the more the amount of negative fixed charge in membrane layer, and the greater the electrical force induced by the electrical field.

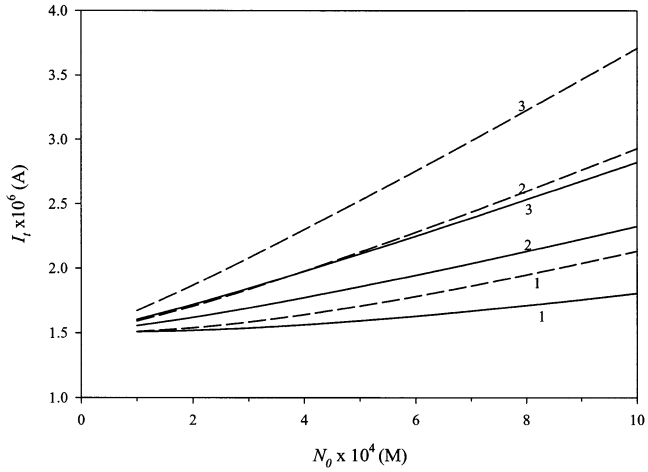

Figure 5. Variation of total current I_t as a function of fixed charge concentration N_0 at various valances of cations. Solid curves, present model, dashed curves, PCM. Curves 1, $a = 1$, $b = 1$; 2, $a = 2$, $b = 1$; 3, $a = 3$, $b = 1$. Key: same as that in Figure 3 except for the values of a, b, and N_0.

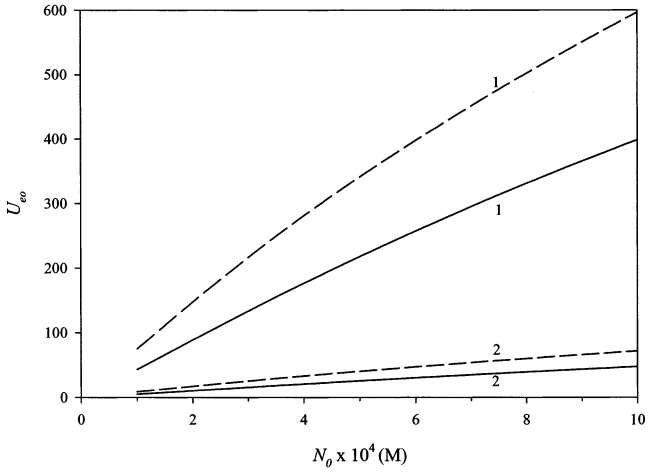

Figure 6. Variation of electroosmotic velocity U_{eo} as a function of fixed charge concentration N_0 at different η^*. Solid curves, present model, dashed curves, PCM. Curve 1, $\eta^* = 1$; 2, $\eta^* = 0.1$. Key: same as that in Figure 3 except for the values of η^* and N_0.

According to Figure 4, the higher the valence of cations, the smaller the V. This is because the membrane is negatively charged, and, therefore, the higher the valence of cations, the greater their shielding effect, which leads to a lower absolute value of potential, and therefore, a smaller u. However, Figure 5 indicates that the higher the valence of cations, the larger the I_t. As can be seen in Figures 4 and 5, the corresponding PCM will overestimate both V and I_t, and the deviation increases with the increase in N_0.

Figure 6 shows the variation of the scaled electroosmotic velocity U_{eo} as a function of the concentration of fixed charge N_0 at different η^*. The electroosmotic velocity is defined as the liquid velocity at a point far away from one of the two plates (by letting $h \rightarrow \infty$) when $P = 0$. As can be seen from Figure 6, for a fixed η^*, U_{eo} increases with N_0, and for a fixed N_0, the smaller the η^* the larger the U_{eo} is. These can be explained by that presented in the discussion of Figures 4 and 5. Figure 6 also indicates that the corresponding PCM will overestimate U_{eo}, and the deviation increases with the increase in N_0.

Figures 7 and 8 illustrate, respectively, the variations in the volumetric flow rate v and the total current I_t as a function of ionic strength I for the case pressure gradient is not applied. As

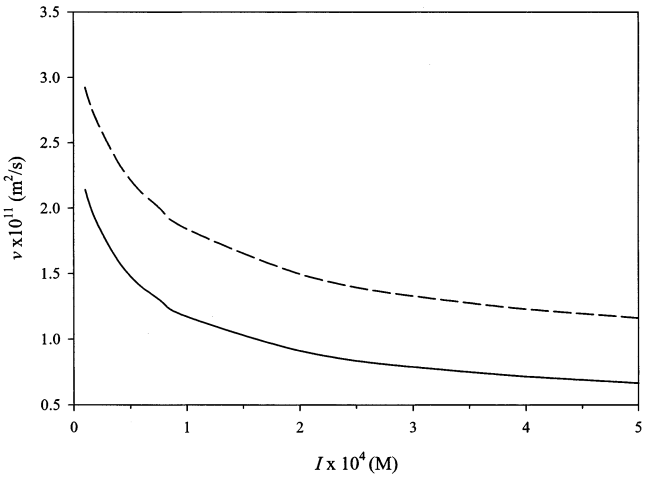

Figure 7. Variation of volumetric flow v as a function of ionic strength I. Solid curves, present model, dashed curves, PCM. Key: same as that in Figure 3 except for the value of I.

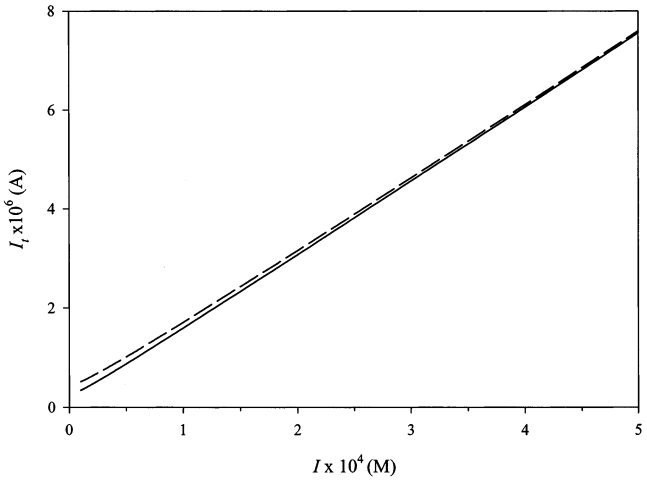

Figure 8. Variation of total current I_t as a function of ionic strength I. Solid curves, present model; dashed curves, PCM. Key: same as that in Figure 3 except for the value of I

can be seen from Figure 7, v decreases monotonically with the increase in I. This is because the higher the ionic strength, the smaller the absolute value of electrical potential, and the less the amount of liquid is driven by the electrical field. However, it is interesting to note that I_t increases monotonically with the increase in I, as suggested by Figure 8. This can be elaborated as follows. The first term on the right-hand side of eq 24 arises from the convective flow of liquid phase, and the second term arises from the diffusion of ions. The former decreases with the increase in I. On the other hand, the latter increases with the increase in I. As can be seen from Figures 7 and 8, the corresponding PCM will overestimate both v and I_t; the deviation of the former is significant, but that of the latter is inappreciable.

The variations of the scaled volumetric flow rate V and the total current I_t as a function of the scaled membrane thickness d at two different friction coefficients f are illustrated in Figures 9 and 10. Here, the total amount of fixed charge in the membrane layer is held constant. As can be seen in Figure 9, for a fixed d, V decreases with the increase in f, as expected. Note that if f is small, V increases with an increase in d, but the reverse is true if f becomes large. This is because if both f and d are small, the fixed charge in the membrane layer is close to the slipping plane, its effect on the flow field is lessened, and the mean liquid velocity becomes smaller. As d gets larger, the

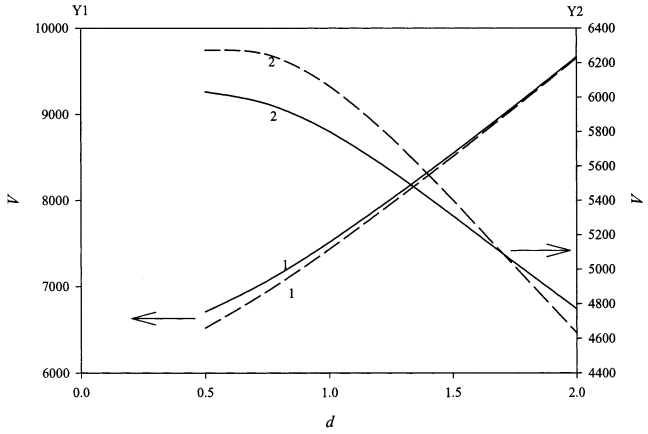

Figure 9. Variation of scaled volumetric flow V as a function of membrane thickness d at various friction coefficient f. Solid curves, present model; dashed curves, PCM. Curve 1 uses X−Y1 axes, $f = 10^{10}$ Ns/m^4, 2 uses X−Y2 axes, $f = 10^{12}$ Ns/m^4. Key: same as that in Figure 3 except for the values of f and d.

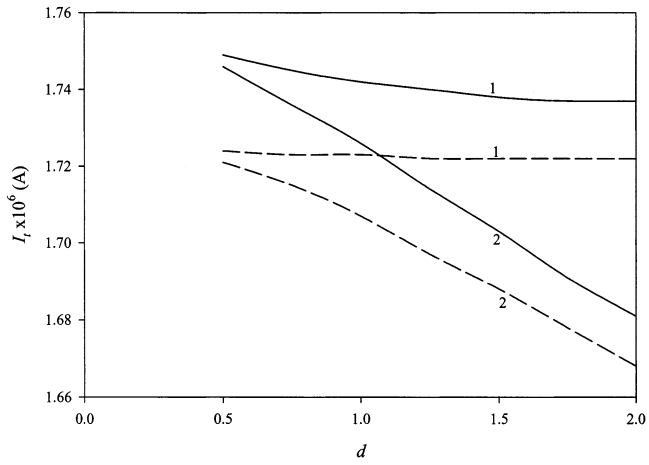

Figure 10. Variation of total current I_t as a function of membrane thickness d at various friction coefficient f. Solid curves, present model; dashed curves, PCM. Curve 1, $f = 10^{10}$ Ns/m^4; 2, $f = 10^{12}$ Ns/m^4. Key: same as that in Figure 3 except for the values of f and d.

fixed charge is dispersed in a wider region in space, its effect on the flow field becomes more significant, and the mean liquid velocity is larger. For the case f is large, the flow of liquid phase is mainly controlled by friction of membrane layer. In this case, since the larger the d, the more important the friction effect, the smaller the mean liquid velocity. Figure 9 indicates that if f is small, the classic PCM will underestimate V; if f is large, the curve predicted by the present model and that by the corresponding PCM intersect at a critical value of d. If a membrane is thinner than this critical value, the PCM will overestimates V, and the reverse is true if it is thicker than the critical value. As can be seen in Figure 10, for a fixed f, the total current I_t decreases with the increase in membrane thickness. However, the variation of I_t as d varies is inappreciable if f is small. Figure 10 also suggests that the corresponding PCM will underestimate I_t, but the deviation decreases with the increase in d.

The variation of the streaming potential E_{st} as a function of the concentration of fixed charge N_0 is shown in Figure 11. Figure 11 reveals that the higher the concentration of fixed charge N_0, the higher the streaming potential E_{st}. This is expected since the larger the N_0, the larger the I_t, and the higher the streaming potential is required to have it balanced. Figure 11 also indicates that the corresponding PCM overestimates the

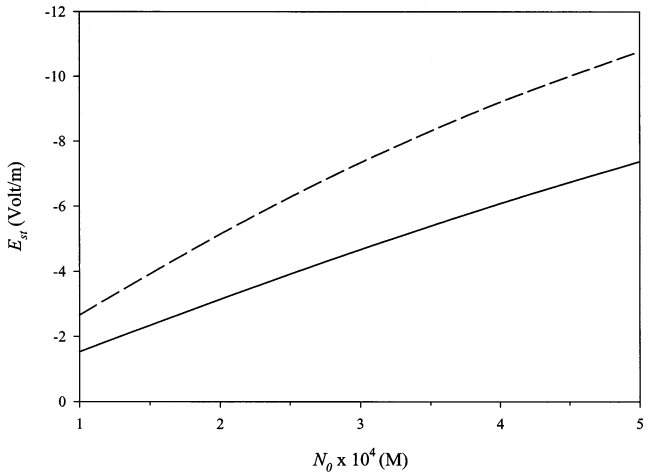

Figure 11. Variation of streaming potential E_{st} as a function of fixed charge concentration N_0 for the case of $P = 10^6$ N/m^3. Solid curves, present model; dashed curves, PCM. Key: same as that in Figure 3 except for the values of P and N_0.

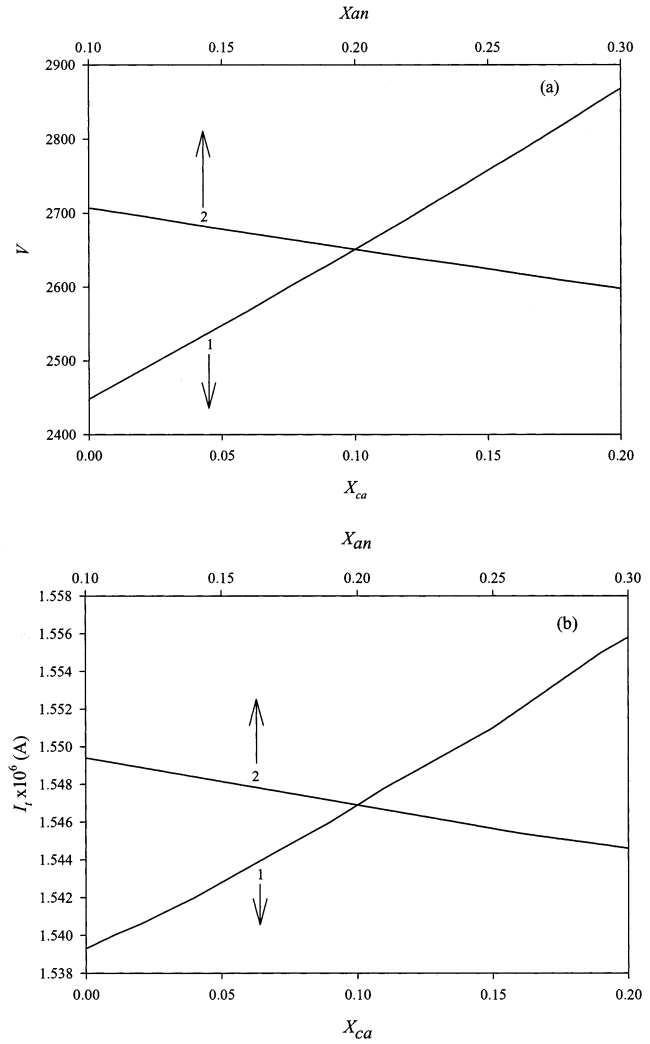

Figure 12. Variation of scaled volumetric flow V (a) and total current I_t (b) as a function of scaled effective radius of cations X_{ca} and anion X_{an} for the case of $f = 10^{12}$ Ns/m^4 and $X_i = 0.3$. Curve 1, $X_{an} = 0.2$; 2, $X_{ca} = 0.1$. Key: same as that in Figure 3 except for the values of X_{ca}, X_{an}, and X_i.

E_{st}, and the deviation increases with the increase in N_0. As illustrated in Figure 3, this is because the classic PCM overestimates the absolute value of electrical potential, which leads to a stronger induced electric field, and, therefore, a higher streaming potential.

Figure 12 shows the variations of the scaled volumetric flow rate V and the total current I_t as a function of the scaled effective radius of cations (counterions) X_{ca} and anions (coions) for a fixed X_i. This figure reveals that both V and I_t increase with the increase in the size of cations. This is because the smaller the counterions the easier for them to present in the membrane layer, which has the effect of lowering the absolute value of electrical potential, thereby leading to a slower liquid velocity. On the other hand, both V and I_t decrease with the increase in the size of anions. Figure 12 indicates that the effect of the size of anions on V and I_t is less significant than that of cations.

4. Summary

A theoretical analysis on the electrokinetic flow of an electrolyte solution in a planar slit, the walls of which are covered by an ion-penetrable charged membrane layer is conducted, taking the effect of the sizes of charged species into account. We conclude that for slits carrying net negative fixed charges, the classic point charge model will overestimate the electrical potential, volumetric flow rate, total current, and streaming potential at a constant membrane thickness; the deviation increases with the increase in N_0 and decrease in the ionic strength. If the sizes of various valences of cations are the same, the following conditions lead to a greater volumetric flow rate: larger concentration of fixed charge, lower valence of cations, smaller ionic strength, larger cations (conterions) size and smaller anions (coions) size. Moreover, the following conditions lead to a greater total current: larger concentration of fixed charge, higher valence of cations, higher ionic strength, larger cations size, and smaller anions size.

Acknowledgment. This work is supported by the National Science Council of the Republic of China.

References and Notes

(1) Hunter, R. J. *Foundations of Colloid Science*; Oxford University Press: Oxford, UK, 1989; Vol. 1.
(2) Dresner, L.; Kraus, K. A. *J. Phys. Chem.* **1963**, *67*, 990.
(3) Burgreen, D.; Nakache, F. R. *J. Phys. Chem.* **1964**, *68*, 1084.
(4) Rice, C. L.; Whitehead, R. *J. Phys. Chem.* **1965**, *69*, 4017.
(5) Sørensen, T. S.; Koefoed, J. *J. Chem. Soc., Faraday Trans. 2* **1974**, *70*, 665.
(6) Hildreth, D. *J. Phys. Chem.* **1970**, *74*, 2006.
(7) Levine, S.; Marriott, J. R.; Robinson, K. *J. Chem. Soc., Faraday Trans. 2* **1975**, 71, 1.
(8) Donath, E.; Voigt, A. *J. Colloid Interface Sci.* **1986**, *109*, 122.
(9) Donath, E.; Voigt, A. *J. Theor. Biol.* **1983**, *101*, 569.
(10) Ohshima, H.; Kondo, T. *J. Colloid Interface Sci.* **1990**, *135*, 443.
(11) Tseng, S.; Kao, C. Y.; Hsu, J. P. *Electrophoresis* **2000**, *21*, 3541.
(12) Keh, H. J.; Liu, Y. C. *J. Colloid Interface Sci.* **1995**, *172*, 222.
(13) Henderson, D.; Blum, L. *J. Chem. Phys.* **1978**, *69*, 5441.
(14) Torrie, G. M.; Valleau, J. P. *Chem. Phys. Lett.* **1979**, *65*, 343.
(15) Valleau, J. P.; Torrie, G. M. *J. Chem. Phys.* **1982**, *76*, 4623.
(16) Bhuiyan, L. B.; Blum, L.; Henderson, D. *J. Chem. Phys.* **1983**, *78*, 442.
(17) Blum, L. *J. Phys. Chem.* **1977**, *81*, 136.
(18) Kjellander, R.; Marcelja, S. *J. Phys. Chem.* **1986**, *90*, 1230.
(19) Kjellander, R.; Akesson, T.; Jonsson, B.; Marcelja, S. *J. Chem. Phys.* **1992**, *97*, 1424.
(20) Gonzalez-Tovar, E.; Lozada-Cassou, M.; Olivares, W. *J. Chem. Phys.* **1991**, *94*, 2219.
(21) Hsu, J. P.; Kuo, Y. C. *J. Chem. Phys.* **1999**, *111*, 4807.
(22) Kuo, Y. C.; Hsu, J. P. *J. Phys. Chem. B* **1999**, *103*, 9743.
(23) Kuo, Y. C.; Hsu, J. P. *Langmuir* **2000**, *16*, 6233.
(24) Hsu, J. P.; Huang, S. W.; Kuo, Y. C.; Tseng, S. *J. Phys. Chem. B* **2002**, *106*, 4269.
(25) Kuo, Y. C.; Hsieh, M. Y.; Hsu, J. P. *Langmuir* **2002**, *18*, 2789.
(26) Huang, S. W.; Hsu, J. P.; Tseng, S. *Electrophoresis* **2001**, *22*, 1881.
(27) Huang, S. W.; Hsu, J. P.; Kuo, Y. C.; Tseng, S. *J. Phys. Chem. B* **2002**, *106*, 2117.